



Gas-liquid mass transfer of carbon dioxide capture by magnesium hydroxide slurry in a bubble column reactor

XIE Peng-fei(谢鹏飞), LI Li-qing(李立清), HE Zhi-cheng(何志成), SU Chang-qing(苏长青)

School of Energy Science and Engineering, Central South University, Changsha 410083, China

© Central South University Press and Springer-Verlag GmbH Germany, part of Springer Nature 2019

Abstract: Magnesium hydroxide ($\text{Mg}(\text{OH})_2$) has been considered as a potential solvent for CO_2 removal of coal-fired power plant and biomass gas. The chemistry action and mass transfer mechanism of CO_2 - H_2O - $\text{Mg}(\text{OH})_2$ system in a slurry bubble column reactor was described, and a reliable computational model was developed. The overall mass transfer coefficient and surface area per unit volume were obtained using experimental approach and simulation with software assistance. The results show that the mass transfer process of CO_2 absorbed by $\text{Mg}(\text{OH})_2$ slurry is mainly liquid-controlled, and slurry concentration and temperature are main contributory factors of volumetric mass transfer coefficient and liquid side mass transfer coefficient. High concentration of CO_2 has an adverse effect on its absorption because it leads to the fast deposition of $\text{MgCO}_3 \cdot 3\text{H}_2\text{O}$ crystals on the surfaces of unreacted $\text{Mg}(\text{OH})_2$ particles, reducing the utilization ratio of magnesium hydroxide. Meanwhile, high CO_3^{2-} ion concentration limits the dissolution of MgCO_3 to absorb CO_2 continually. Concentration of 0.05 mol/L $\text{Mg}(\text{OH})_2$, 15% vol CO_2 gas and operation temperature at 35 °C are recommended for this CO_2 capture system.

Key words: mass transfer; CO_2 capture; magnesium hydroxide; bubble column

Cite this article as: XIE Peng-fei, LI Li-qing, HE Zhi-cheng, SU Chang-qing. Gas-liquid mass transfer of carbon dioxide capture by magnesium hydroxide slurry in a bubble column reactor [J]. Journal of Central South University, 2019, 26(6): 1592–1606. DOI: <https://doi.org/10.1007/s11771-019-4115-6>.

1 Introduction

CO_2 has attracted global attention on climate change and been widely discussed as a special kind of pollutant. Coal-fired power plant and biomass gas are the main sources of carbon dioxide emissions, different fuel varieties and carbon contents lead to the difference of CO_2 partial pressure in flue gas. The proportion of CO_2 in the flue gas of coal-fired power plants accounts for 10%–20% and biomass gas for 12%–30%, which is adverse to combustion and decreases calorific value [1, 2]. In these carbon capture and sequestration (CCS) technologies, chemical absorption is

regarded as the most direct and efficient way [3]. Monoethanolamine (MEA), ammonia and potassium carbonate (K_2CO_3) are common absorbent selections for CO_2 capture, but they all have defects of varying degrees, such as the corrosivity and toxicity of MEA solution and high energy consumption [4], high running cost [5], the high volatile nature of ammonia [6] and the precipitation of ammonia carbonate salts [7]. Academia and industry are still studying new decarbonizing agents with low energy consumption, high capture rate and low cost. $\text{Mg}(\text{OH})_2$ is referred as CO_2 capture agent for its low price, relatively low energy consumption and property of not easy to encrust [8].

Foundation item: Project(21878338) supported by the National Natural Science Foundation of China; Project(2015BAL04B02) supported by the National key Technology R&D Program of China; Project(2018K2038) supported by the key Research and Development Project of Hunan Province, China; Project supported by Hunan Collaborative Innovation Center of Building Energy Conservation & Environmental Control, China

Received date: 2018-01-10; **Accepted date:** 2019-01-23

Corresponding author: LI Li-qing, PhD, Professor; Tel: +86-13807483619; E-mail: liqingli@hotmail.com; ORCID: 0000-0001-8297-309X

Wet magnesium method decarbonization technology is derived from limestone and dolomite wet desulphurization technology in flue gas desulfurization (FGD) [8]. Its basic principle is that $\text{Mg}(\text{OH})_2$, as decarbonization agent, absorbs carbon dioxide and converts it into magnesium bicarbonate solution, which is heated in the desorption tower to regenerate magnesium hydroxide over and over again. The bubble column reactor is widely used for mass transfer and chemical reactions of wet magnesium method decarbonization because of its simple structure and excellent performance [9]. Through gas bubbler installed at the bottom of the bubble column, CO_2 gas is dispersed into small bubbles, then reacts with $\text{Mg}(\text{OH})_2$ slurries to enhance the absorption efficiency, which is equivalent to reducing mass transfer resistance when it applies to industrial production. Therefore, it is essential to study the mass transfer process of the $\text{CO}_2\text{-H}_2\text{O-Mg}(\text{OH})_2$ system. In general, the presence of chemical reactions will enhance mass transfer of the liquid-solid interface, and gas-liquid interfacial mass transfer becomes the determining step of the transfer process [10]. A continuous bubble column scrubber was used to capture CO_2 gas by using a NaOH solution under a constant pH operation, the higher values of overall mass-transfer coefficient and absorption efficiency were required to give smaller gas-liquid molar rate ratio [11]. Absorption of CO_2 into Piperazine (Pz) solution was investigated by PASHAEI et al [12], total gas phase mass transfer coefficient (K_g) and liquid side mass transfer coefficient increases with the Piperazine concentration and CO_2 partial pressure. Most studies on the mass transfer behavior were limited to determine the volumetric mass transfer coefficient, K_{ga} . Nevertheless, the volumetric mass transfer coefficient was not enough to describe the mass transfer mechanism [13]. Further, the calculation of mass transfer rate and specific surface area of phase boundary is helpful to understand the limiting factors of mass transfer process.

Therefore, the purpose of this study is to 1) investigate the gas-liquid mass transfer mechanism with chemical reactions in the absorption process of $\text{CO}_2\text{-H}_2\text{O-Mg}(\text{OH})_2$ system, 2) calculate the gas/liquid side mass transfer coefficient for determining which resistance controls, and 3) evaluate the influences of different reaction

conditions on the absorption rate.

2 Experimental

The absorption experimental setup consisted of five parts: 1) simulated gas generation; 2) flow control; 3) bubble column reactor; 4) gas sampling and analysis; 5) data acquisition. The experimental setup is shown schematically in Figure 1.

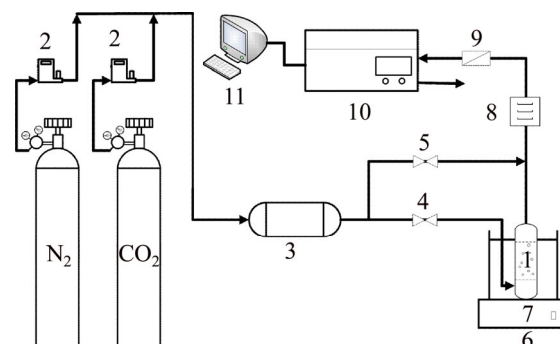


Figure 1 Schematic of experimental setup (1—Bubble column; 2—Mass flow controller; 3—Buffer gas bottle; 4—Valve; 5—Valve; 6—Water bath; 7—Magnetic stirrer; 8—Dryer; 9—Filter; 10—NDIR CO_2 analyzer; 11—Data acquisition system)

A cylindrical glass vessel with height of 27 cm, diameter of 7 cm was used as the main body of bubble column reactor. The bubble column was placed in an electro-thermostatic water bath, and sat on the magnetic stirrer which allowed magnetic mixing to be applied to the fluid inside the column. A porous plate gas distributor (pore size 0.5–3 mm) was installed at the bottom of the column as the gas bubbler.

The simulated gas was produced by mixing pure N_2 gas with pure CO_2 gas (high purity >99.99%, Changsha Gaoke Gas Inc., China). Both gas streams were controlled by mass flow controllers to get required CO_2 concentrations. Then the gas stream was charged into a buffer gas bottle in order to be well mixed and minimize the fluctuation of the gas pressure. The $\text{Mg}(\text{OH})_2$ (reagent class, purity >98%, Xilong Chemistry Inc., China) slurries in the bubble column were maintained at 1 L, and the gas volumetric flow rate was maintained at 1 L/min. The outlet gas absorbed by the bubble firstly passed through an ice-salt bath to remove water vapor, then all particles were removed by a filter before the gas stream went into the infrared gas analyzer (Gasboard-3100, Suzhou

Chemical Engineering Instrument Inc., China; range: CO₂ 0 to 50 vol%; accuracy ±1% of full-scale; repeatability error: ≤1%; recommended gas flow rate: 0.7–1.2 L/min). The infrared gas analyzer was periodically calibrated before every set of experiments.

Table 1 Experiment conditions

Parameter	Value
Absorption temperature/°C	20–50
Gas flow rate/(L·min ⁻¹)	1
Bubble column size/cm	7×28
Inlet CO ₂ concentration/%	15–30
Mg(OH) ₂ concentration/(mol·L ⁻¹)	0.025–0.1
Agitation rate/(r·min ⁻¹)	1000
Orifice diameter of gas distributor/mm	0.5–3

The viscosity and surface tension of Mg(OH)₂ slurries were measured by using Engler viscometer (RPNE-1A, Ruipu Instrument Inc.) and automatic tension tester (JK99B, Shanghai Powereach Inc.). The Engler viscosity refers to the ratio of time, which is a certain volume of sample flowing out from viscometer with that of distilled water at 20 °C. Each data was measured three times and averaged.

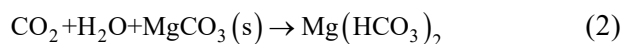
The results showed that the viscosity and surface tension of Mg(OH)₂ slurries are similar to that of distilled water within the operating conditions of this experiment (temperature 20–50 °C, Mg(OH)₂ concentration 0.025–0.1 mol/L).

3 Mass transfer model

3.1 Reaction mechanism of CO₂-H₂O-Mg(OH)₂ system

The absorption process is generally represented as two steps: Mg(OH)₂ slurries absorbs

CO₂ and converts it into MgCO₃, and MgCO₃ further absorbs CO₂ and converts it into Mg(HCO₃)₂. The following overall reactions are given:



Although the overall reactions are simple, the chemistry is quite complex. The sequence of all the ionic reactions involved is as follows:

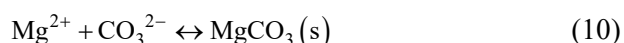
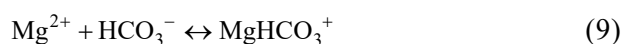
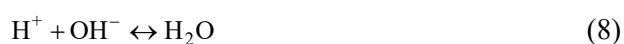
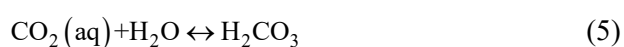
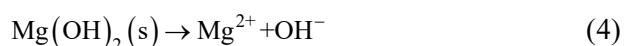


Figure 2 demonstrates the mass transfer schematic of the system. Turbulent flow fully develops within the mainstream; as a result, the mainstream has a constant concentration of substances. The turbulence slowly reduces within turbulent boundary layer where mass is transferred totally by turbulent eddy. In the stagnation layer which is closer to the interface, turbulent eddy has become so weak that the momentum provided by molecular viscosity passes it, and the flow tends to become laminar flow. However, much of mass transfer inside of this layer is still depending on turbulent diffusion because of the fact that the molecular diffusion coefficient is typically three orders for magnitude smaller than the eddy diffusion coefficient. Only in the diffusion layer, the molecular diffusion dominates the mass transfer.

Table 2 Viscosity and surface tension of Mg(OH)₂ slurries under different experiment conditions

Temperature/°C	Mg(OH) ₂ concentration/(mol·L ⁻¹)	Dropping time/s	Engler viscosity (°E)	Kinematic viscosity/(m ² ·s ⁻¹)	Surface tension/(10 ⁻³ N·m ⁻¹)
20	0.1	51.9	1.02	1.17	73.14
25	0.025	51.1	1.00	1.00	71.99
25	0.05	51.3	1.01	1.08	72.03
25	0.1	52.4	1.03	1.25	72.16
35	0.1	50.5	0.99	0.92	70.57
50	0.1	48.9	0.96	0.67	67.95

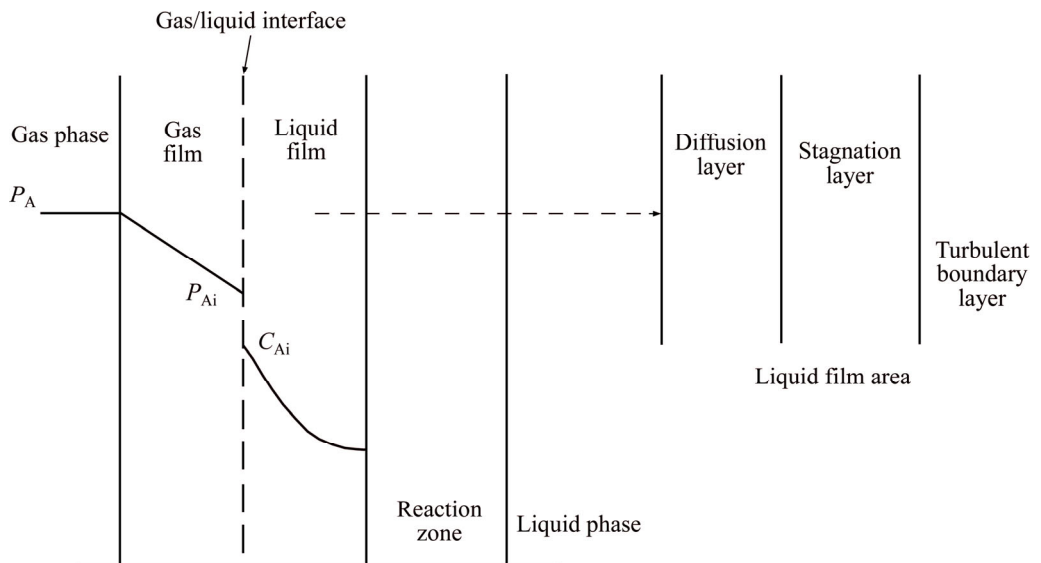


Figure 2 Mass transfer schematic of CO₂-H₂O-Mg(OH)₂ system

Assign c for concentration of solute, y for the distance perpendicular to the interface. Thus, their correlations are given as follows [14]:

- 1) Turbulent boundary layer: $c \propto \ln y$
- 2) Stagnation layer: $c \propto 1/y^3$
- 3) Diffusion layer: $c \propto y$

These correlations reveal the fact that the mass flux is proportional to zero power of the diffusion coefficient ($N_a \propto D^0$) in the outboard film, and is proportional to diffusion coefficient ($N_a \propto D^{1.0}$) near the interface. So n is supposed to lay between 0 and 1 when it applies D^n to correlate the real mass transfer process [15].

3.2 Volumetric mass transfer coefficient $K_G a$

The model is based on the main assumptions: the components (magnesium hydroxide particles) in the liquid phase are uniformly distributed and bubble flow regime is uniform bubble flow. Overall mass transfer coefficient can be expressed in terms of the ratio of absorption rate and driving force:

$$r_a = \frac{N_a}{V_1 t} = K_g a (P_{\text{average}} - P_{cl}^*) = K_l a (C_{\text{average}} - C_{cl}) \quad (11)$$

The absorption rate equation can be expressed as follows:

$$r_a = k_g a (P_{\text{average}} - P_i) = k_l a (C_i - C_{cl}) \quad (12)$$

where C_i and P_i are CO₂ concentrations at the gas-liquid interface following the Henry's law.

$$H_{\text{CO}_2} = \frac{C_i}{P_i} \quad (13)$$

In the formula, C_{cl} and P_{cl}^* are defined as the concentration and corresponding partial pressure on CO₂ in the bulk liquid. P_{average} is the average partial pressure on CO₂ in the bulk gas inside bubbles.

The CO₂ partial pressure in the bubble is reduced as the bubble rising through the column. Although the bubble stays in the bubble column for a short time, the partial pressure on carbon dioxide in the main gas phase of the bubbling process cannot be regarded as a fixed value to simplify the calculation because of the high absorption rate of the early stage of the absorption process and the large pressure drop in the outlet carbon dioxide partial pressure compared with the import. Here, it is assumed that the drop of pressure is lineal. The inlet CO₂ partial pressure is invariant, and the outlet CO₂ partial pressure changes with respect of time. For mean mass transfer coefficient, it is the mean CO₂ partial pressure on the absorption time that we concern. As the imported CO₂ concentration is constant, $\overline{P_{\text{out}}}$ is defined as the time-averaged value of $P_{\text{out},\tau}$, as follows:

$$\overline{P_{\text{out}}} = \frac{1}{t} \int_0^t P_{\text{out},\tau} d\tau \quad (14)$$

So, P_{average} can be written as:

$$P_{\text{average}} = \frac{P_{\text{in}} + \frac{1}{t} \int_0^t P_{\text{out},\tau} d\tau}{2} \quad (15)$$

To represent the mass transfer driving force, the derivation begins with calculating C_{cl} , the concentration of free CO₂ molecule in the liquid

phase at the absorption equilibrium.

Assign y_1 and y_2 for the CO_2 concentration of inlet and outlet gas, the absorption efficiency η can be written as:

$$\eta = \frac{y_1 - y_2}{y_1} \times 100\% \quad (16)$$

Draw the fitting curve of η , the total amount of absorbed CO_2 may be integrated as:

$$N_a = Ny_1 \int_0^t \eta_\tau d\tau \quad (17)$$

Knowing the amount of $\text{Mg}(\text{OH})_2$ and CO_2 , an OLI analyzer was introduced to simulate the concentration of each component at each moment during the absorption process. So C_{cl} is obtained.

Then, Eq. (11) can be rewritten as:

$$r_a = K_g a \left(\frac{P_{in} + \frac{1}{t} \int_0^t P_{out,\tau} d\tau}{2} - \frac{C_{cl}}{H_{\text{CO}_2}} \right) \quad (18)$$

Finally, the volumetric mass transfer coefficient $K_g a$ can be determined.

3.3 Bubble behavior

As shown in Figure 3, the geometry and size of bubble swarms differ with respect to the position in the liquid column. At the bottom of column, the simulated gas enters the liquid through nozzles of the gas distributor, forming large bubbles with shapes of ellipsoidal and spherical-cap. Large bubbles tend to break up into smaller bubbles, and small bubbles tend to join together [16]. There exists an equilibrium between breakage and

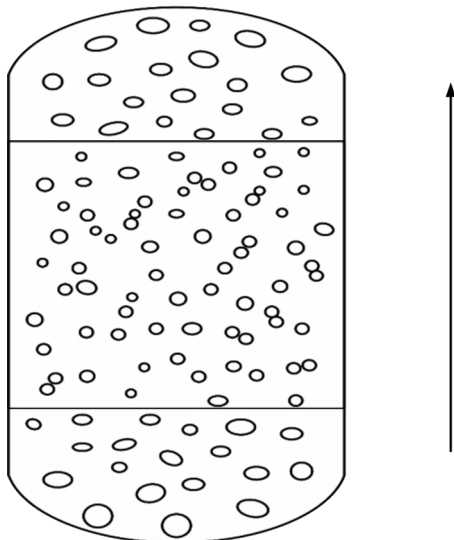


Figure 3 Distribution plot of bubble swarms

coalescence of rising bubbles [17]. Generally, large bubbles make up the majority of the bottom and top region of the column, while small bubbles congested the middle part of the vessel. And in most cases the distribution of bubble size approximately follows the logarithmic normal distribution law [18].

There have been many researches on the breakage and coalescence behaviors of bubbles, and it is also found that agitation rate and superficial gas velocity affect a lot. In general, a high agitation rate results in a sharp drop in the mean bubble size, whereas, a high superficial gas velocity reduces the effect [19]. To figure out the sauter mean diameter of bubble swarms for subsequent calculating, the whole situation of bubble behavior needs to be investigated and analyzed.

Photography & image analysis and radiography are mainstream experimental ways to detect the bubble size [20]. These optical measurements require transparent wall and liquid and low gas holdup, while $\text{Mg}(\text{OH})_2$ slurry is milky white and the gas holdup is relatively high. Optical measurements also provide bubble profile in wall region mainly, so it is inadequate to be utilized to calculate the sauter mean value of bubble swarms considering the radial distribution of bubble size caused by turbulence and wall effect, especially in small scale reactors [21]. GADDIS et al [22] derived a well-accepted formula from strict force analysis to calculate the initial bubble diameter which just generated from gas distributor under low and moderate gas pressures:

$$d_0 = \left[\left(\frac{6d_h \sigma}{\rho_l g} \right)^{4/3} + \left(\frac{81\nu V}{\pi g} \right) + \left(\frac{135V^2}{4\pi^2 g} \right)^{4/3} \right]^{1/4} \quad (19)$$

It is found that the second addend (viscosity and flow rate) decides the initial bubble diameter. The numerical value of the second addend is three orders for magnitude larger than the rest two addends according to experimental data. In other words, nozzle diameter has barely any influence on bubble size. The initial bubble diameters in this experiment are about 14 mm.

On account of wall effect and gas holdup which affect bubble breakage and coalescence, a semi-empirical correlation to estimate sauter mean bubble radius under dense bubbling conditions has been proposed [14]:

$$r_b = 2.56h^{-0.2} \left(\frac{\sigma}{\rho_l \rho} \right)^{0.6} \left(\frac{v_g}{v_l} \right)^{0.25} \frac{\varepsilon^{0.65}}{(1-\varepsilon)^{0.4}} \quad (20)$$

The gas holdup in electrolyte solutions cases, ε is estimated according to Eq. (21) suggested by AKITA et al [23]:

$$\frac{\varepsilon}{(1-\varepsilon)^4} = 0.25 \left(\frac{gD^2 \rho_l}{\gamma} \right)^{1/8} \left(\frac{gD^3}{v^2} \right)^{1/12} \left(\frac{U_g}{\sqrt{gD}} \right)^{1.0} \quad (21)$$

The sauter mean bubble diameters of bubble swarms in this experiment are about 2 mm.

With the mean diameter, the characteristic exposure time θ can be estimated if bubble rising velocity is known according to its definition. After detachment from the orifice, bubble would have a brief amount of time to accelerate before it reaches the terminal rising velocity. It is reported that air bubble needs to climb about 10–20 mm in distilled water [17]. Concerning that this period of time is too short, it is assumed that bubbles are rising at a uniform velocity, which is equal to the terminal rising velocity. The rise of a bubble in liquid is a function of several parameters [24], including bubble characteristics (size and shape), properties of gas-liquid systems (density, viscosity, surface tension, concentration of solute, density difference between gas and liquid), liquid motion and operating conditions. Many correlation researches have been reported in the past decades, Mendelson proposed the well-accepted wave theory for prediction of bubble rises velocity, then derived a simple but efficient formula based on published data [25].

$$U_r = \sqrt{\frac{\sigma}{r_b \rho_l} + gr_b} \quad (22)$$

This equation has shown very good agreement with the experimental data onto Newtonian fluids except for very small bubbles (<0.5 mm). As mentioned earlier, the magnesium hydroxide slurries present almost the same flow characteristics as distilled water, so it is feasible to treat those slurries as Newtonian fluids. Figure 4 demonstrates how the terminal bubble rise velocity would change with respect of bubble radius under certain liquid surface tension and density in our experiments. As shown, the trend of rise velocity does not simply increase linearly when bubble size gets larger, but it is similar to the hook shape which is decreasing first and then increasing. When the bubble radius is

about 3 mm, the minimum rise velocity is obtained, which is about 0.23 m/s. The velocity may correspond to two different bubble sizes which lie exactly in the recommended bubble size region. Moreover, the size range falls within the range of 1–16 mm in diameter, which covers the size range of common bubbles in bubble experiment. Therefore, it is suitable to predict rise velocity through bubble size rather than reverse it [26]. Otherwise, it will get into dilemma to predict the gas-liquid interfacial area.

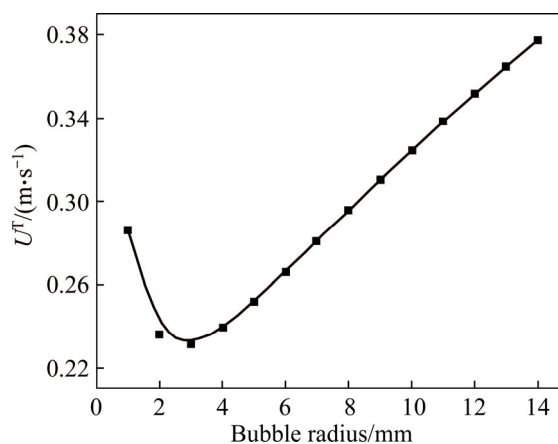


Figure 4 Relationship between bubble radius and terminal rising velocity in CO₂-H₂O-Mg(OH)₂ system

3.4 Mass transfer coefficient

According to the original penetration model, the liquid phase mass transfer coefficient (K_1) correlates with the diffusion coefficient (D_1) of solute and characteristic contact time θ . θ is the time which takes for the liquid around the bubble to be completely replaced, specifically, the time it takes for the bubble to rise a bubble’s diameter. Therefore, the correlations are given as:

$$\theta = \frac{d_b}{U_t} \quad (23)$$

According to the mass transfer model based on penetration theory, K_1 is given as:

$$k_1 = 2\sqrt{\frac{D_1}{\pi\theta}} \quad (24)$$

Notably, this correlation does not take chemical reaction into account, Eq. (24) cannot be used to calculate K_1 directly in the system of CO₂-H₂O-Mg(OH)₂ in this experiment. The specific gas-liquid interfacial area, a , is the total interfacial area per unit volume of liquid (without bubbles). Introducing the concept of gas holdup, ε , the

specific gas-liquid interfacial area has a simple formula which can be easily deduced with knowing the bubble size.

$$a = \frac{V_g}{V_l} = \frac{6\varepsilon}{d_b(1-\varepsilon)} \quad (25)$$

According to its concept, V_g is defined as the actual gas volume in the bubble column, V_t is defined as the total inlet gas volume throughout the absorption process, V_l is defined as the actual liquid volume in the bubble column, then:

$$V_g = V_t \frac{\theta}{t} \quad (26)$$

Substituting the volume and superficial area of single bubble, a can be calculated as:

$$a = \frac{V_g}{V_l} = \frac{6V_t\theta}{d_b V_l t} \quad (27)$$

Overall mass transfer coefficient of K_g is given as:

$$K_g = \frac{H_{CO_2} r_a d_b (1-\varepsilon)}{3\varepsilon \left[H_{CO_2} \left(P_{in} + \frac{1}{t} \int_0^t P_{out,\tau} d\tau \right) - 2C_{cl} \right]} \quad (28)$$

According to the additive property of mass transfer resistance, the overall mass transfer resistance is summed by the separate side resistances.

$$\frac{1}{K_g} = \frac{1}{k_g} + \frac{1}{H_{CO_2} k_l} \quad (29)$$

Assume that the bubble geometry is rigid sphere, the mass transfer inside the bubble and gas film is investigated, the theoretical equation for diffusing to the spherical surface is [27]:

$$\frac{\partial C}{\partial \tau} = D_g \frac{\partial^2 C}{\partial r_B^2} + \frac{2}{r} \frac{\partial C}{\partial r_B} \quad (30)$$

This expression can be solved under proper boundary conditions and transform the solution into expression using dimensionless number:

$$N_{Sh} = \frac{k_g d_b}{D_g} = \frac{1}{6N_{Fo}} \left[1 - \frac{6}{\pi^2} \exp(-4\pi^2 N_{Fo}) \right] \quad (31)$$

The contact time θ is taken as the ratio of bubble size to gas rising velocity and substituted into Eq. (23), then N_{Fo} is the reciprocal of N_{Pe} . Due to the considerable deviation from counting k_g when N_{Pe} is small, an additional item was suggested to adding in the formula. Rewrite Eq. (31) as:

$$N_{Sh} = \frac{k_g d_b}{D_g} = 6.6 + \frac{1}{6} N_{Pe} \left[1 - \frac{6}{\pi^2} \exp(-4\pi^2 / N_{Pe}) \right] \quad (32)$$

Because of N_{Pe} is relatively small (Generally two or three orders of magnitude smaller than 6.6 in this experiment), SUH et al [28] suggested removing the complicated item and get the gas phase mass transfer coefficient:

$$k_g = \frac{6.6 D_g}{d_b} \quad (33)$$

What has to be mentioned is that the k_g above is measured in cm/s. The above equation is divided by the gas constant and temperature to unify the calculating units of Eq. (29):

$$k_g = \frac{6.6 D_g}{d_b R T} \quad (34)$$

The diffusion coefficient of gas mixture, D_g , is estimated using the following semi-empirical formula [29]:

$$D_g = \frac{1.517 T^{1.81} \left(\frac{1}{M_A} + \frac{1}{M_B} \right)^{0.5}}{p (T_{ca} T_{cb})^{0.1405} (V_{ca}^{0.4} + V_{cb}^{0.4})^2} \quad (35)$$

Liquid side mass transfer coefficient (k_l) was obtained by substituting Eq. (27) into Eq. (22), as follows:

$$k_l = \left[6.6 d_b D_g r_a (1-\varepsilon) \right] / \left\{ 19.8 \varepsilon D_g \left[H_{CO_2} \left(P_{in} + \frac{1}{t} \int_0^t P_{out,\tau} d\tau \right) - 2C_{cl} \right] - d_b^2 H_{CO_2} R T r_a (1-\varepsilon) \right\} \quad (36)$$

The whole scheme of the model computation is explained as Figure 5.

4 Results and discussion

4.1 Effect of Mg(OH)₂ concentration

To investigate the influence of Mg(OH)₂ concentration on CO₂ the absorption, 0.025, 0.05, 0.1 mol/L Mg(OH)₂ slurries and 15 vol% CO₂ gas under 25 °C were conducted in this experiment. The CO₂ absorption capacity of slurry with different concentration is shown in Figure 6(a). The time for the Mg(OH)₂ slurry to reach the absorption equilibrium becomes longer as the concentration

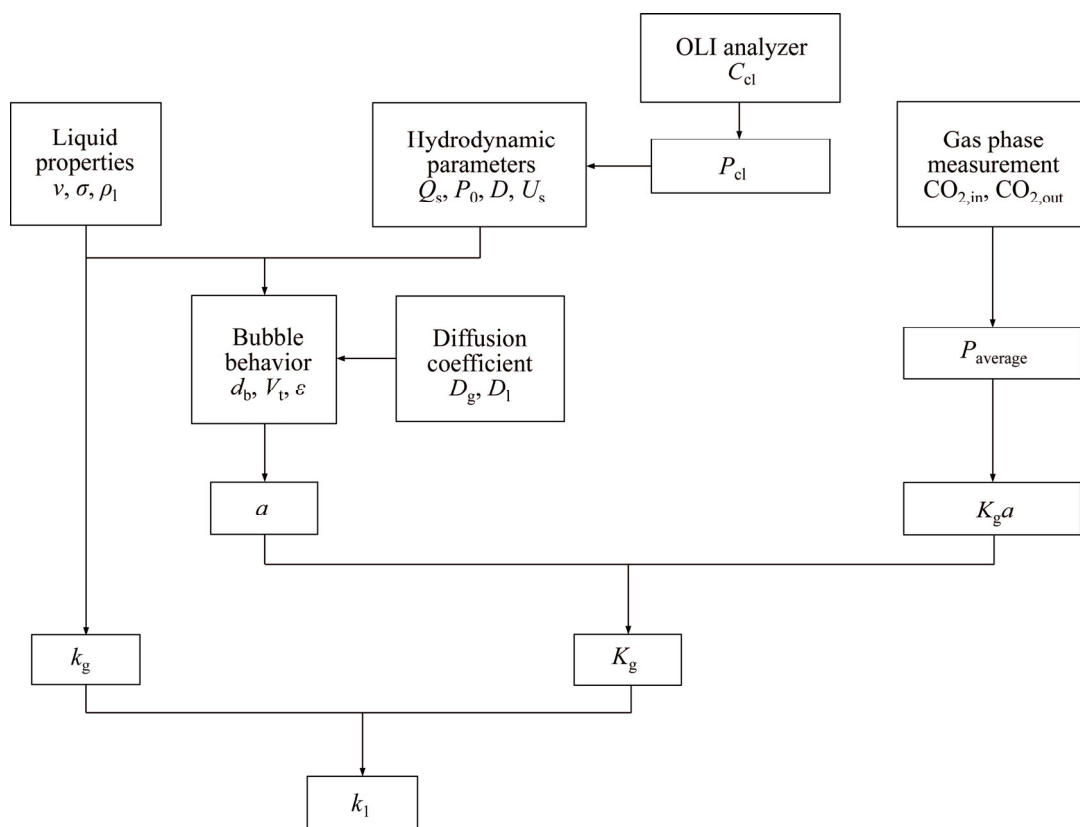


Figure 5 Schematic of computational model

of slurry increases, and the total amount of carbon dioxide that could be absorbed also increased. Figure 6(b) shows the control groups of outlet CO₂ partial pressure. First, the partial pressure decreased sharply due to the rapid neutralization reaction of dissolved Mg(OH)₂ and CO₂, and then MgCO₃ was formed. In addition, after the dissolved OH⁻ ions were consumed, the Mg(OH)₂ particles in the slurry began to dissolve and the outlet CO₂ partial pressure kept at low level. Last, after the Mg(OH)₂ was consumed, MgCO₃ began to dissolve and continued to absorb CO₂, generating soluble Mg(HCO₃)₂. The outlet CO₂ partial pressure kept rising until the dissolved ions reached their solubility product. When the concentration of Mg(OH)₂ increased from 0.025 to 0.05 mol/L, the absorption capacity of slurry to CO₂ was also doubled, which was from 0.04 to about 0.08 mol/L. However, the amount of CO₂ absorbed per liter of slurry was only increased by about 0.04 mol when the concentration of Mg(OH)₂ was doubled from 0.05 to 0.1 mol/L. It can be seen that the increase in the absorption capacity of CO₂ caused by the increase in Mg(OH)₂ is a linear increase in the low concentration range of Mg(OH)₂. When the slurry

concentration exceeds 0.05 mol/L, the increase in carbon absorption capacity decreases. Regarding to change in mass transfer rate, as the concentration of Mg(OH)₂ slurry increases, the volume mass transfer coefficient (K_ga) increases and then remains stable, the variation trend of liquid phase mass transfer coefficient k₁ is similar to volume mass transfer coefficient. The change trend of gas mass transfer coefficient k_g is different from the former two. 0.025 and 0.1 mol/L of Mg(OH)₂ slurry have almost the same gas mass transfer coefficient, and the minimum value of k_g is obtained at the slurry concentration of 0.05 mol/L. The mass transfer resistance is the reciprocal of mass transfer coefficient. By comparing the absolute value of the gas mass transfer resistance and the liquid mass transfer resistance, it can be found that the mass transfer resistance is mainly concentrated in the liquid phase. Therefore, less mass transfer resistance means greater liquid phase mass transfer coefficient. Considering carbon absorption ability, equilibrium time and the mass transfer rate, the decarburization optimal concentration of Mg(OH)₂ slurry is 0.05 mol/L under ambient temperature (25 °C).

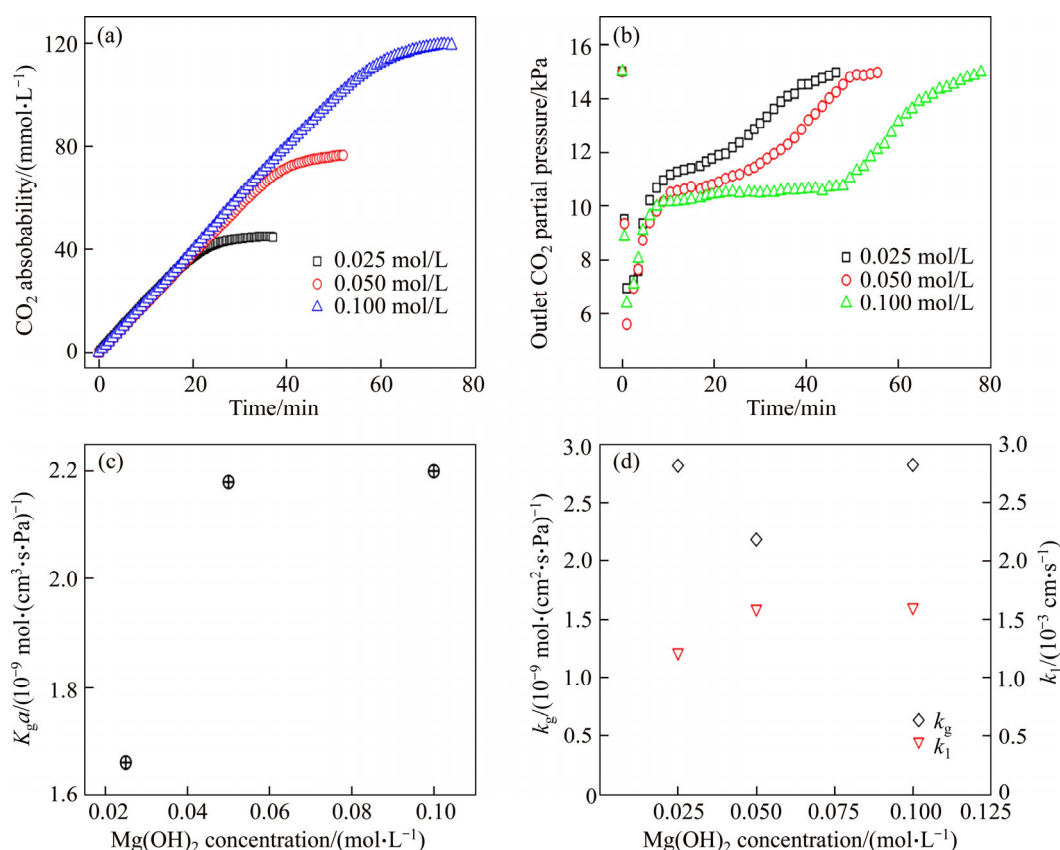


Figure 6 Absorption of CO₂ under 15 vol% CO₂, 25 °C conditions at different concentrations of Mg(OH)₂ slurries: (a) CO₂ absorption capacity; (b) Outlet CO₂ partial pressure; (c) Volumetric mass transfer coefficient; (d) Gas/liquid phase mass transfer coefficients

4.2 Effect of CO₂ concentration

To investigate effect of CO₂ concentration on the decarbonization absorption and mass transfer of Mg(OH)₂, 0.05 mol/L Mg(OH)₂ slurries and simulated biomass gas containing 10%, 15%, 20%, 25%, 30% (volume fraction) CO₂ under 25 °C were conducted. As shown in Figure 7, there are significant differences between low CO₂ concentration control groups (10% and 15%, volume fraction) and high CO₂ concentration control groups (20%–30%, volume fraction). Low CO₂ concentration has more advantages in carbon absorption capacity and mass transfer rate. According to Eqs. (1) and (2), 0.05 mol Mg(OH)₂ absorbs 0.1 mol CO₂ when it completely transforms into Mg(HCO₃)₂. The absorbability of high CO₂ concentrations groups is below 0.05 mol/L, which means there are still some unreacted Mg(OH)₂. This is supported by OLI analysis data. The amount of Mg(OH)₂ not involved in the reaction at the absorption balance is 0.010, 0.007 and 0.013 mol, respectively when the concentration of CO₂ gas is 20%, 25% and 30% (volume fraction) respectively.

The reason for this phenomenon is that high CO₂ concentration gas leads to high concentration of CO₃²⁻ ions in the solution, which requires less Mg²⁺ ions to reach the solubility product. According to nucleation theory, the Mg(OH)₂ particles are deactivated by the covering of MgCO₃·3H₂O crystals. The fast deposition of crystals blocks the dissolution of Mg(OH)₂ and increase the mass transfers resistance on the solid-liquid phase. This also explains the sharp decrease of CO₂ absorption efficiencies of high gas concentration. The driving force for gas-liquid phase mass transfer process increases from 8.11×10^3 to 2.84×10^4 Pa when CO₂ concentration rises from 10 vol% to 30 vol%. Even so, the volumetric mass transfer coefficient $K_g a$ and liquid mass transfer coefficient k_1 are higher under the condition of low concentration CO₂ than under the condition of high concentration CO₂, except that the mass transfer coefficient of gas is basically constant k_g . Although the absorption equilibrium time of CO₂-H₂O-Mg(OH)₂ system under the condition of 15 vol% CO₂ concentration is about two-thirds of that of 10 vol% CO₂ concentration,

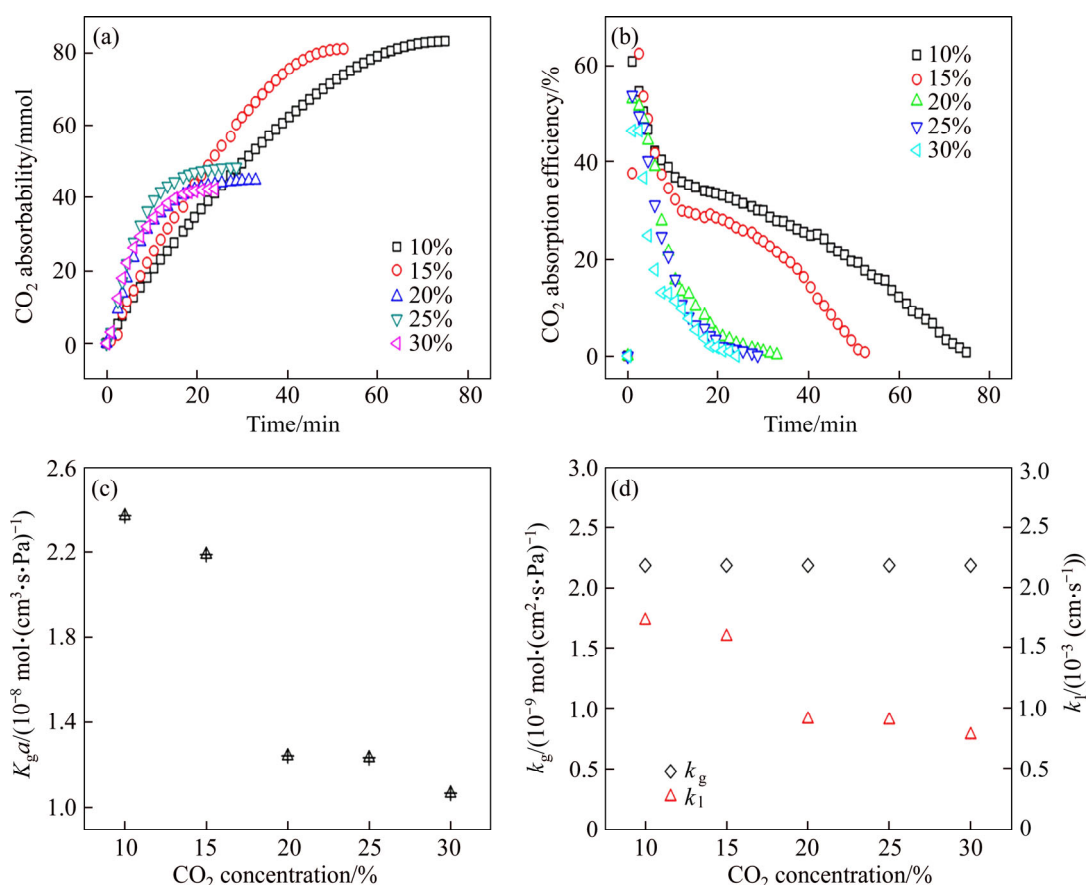


Figure 7 Absorption of CO₂ under 0.05 mol/L Mg(OH)₂, 25 °C conditions with different concentrations of CO₂: (a) CO₂ absorption capacity; (b) CO₂ absorption efficiency; (c) Volumetric mass transfer coefficient; (d) Gas/liquid phase mass transfer coefficients

the volumetric mass transfer coefficient (K_{ga}) and liquid phase mass transfer coefficient (k_l) calculated by the former decreased by 7.6% and 5.9% respectively compared with the latter, because the increase of mass transfer driving force is greater than the decrease of absorption equilibrium time. Combining decarbonization capacity, absorption equilibrium time and mass transfer rate, 15% is the optimal CO₂ concentration for decarbonization using Mg(OH)₂ slurry.

4.3 Effect of temperature

Temperature usually plays an important role in chemical absorption. To ensure abundant supply of reactants, 0.1 mol/L Mg(OH)₂ slurries and 30 vol% CO₂ gas under 20, 35 and 50 °C were conducted in this experiment. Figure 8(a) shows the decarbonization capacity of Mg(OH)₂ slurry at different temperatures. As shown in the absorption curve, the decarbonization capability of Mg(OH)₂ slurry at different temperatures is not much

different. Mg(OH)₂ slurry under 20 °C absorbs the maximum amount of CO₂, which is about 0.122 mol/L, and others were 0.111 and 0.118 mol/L respectively under 35 and 50 °C. In addition, the outlet partial pressure curves of carbon dioxide are consistent under 20 and 50 °C, which is significantly higher than the condition of 35 °C in the first half of the reaction. This means that the latter absorbs more CO₂. More specifically, the volumetric mass transfer coefficient K_{ga} under 35 °C is appreciably higher than the other two groups, as shown in Figure 8(c). K_{ga} and k_l increase with temperature rising in low temperature range (20–35 °C), while the trends reverse in high temperature range (35–50 °C). Note that the volumetric mass transfer coefficient (K_{ga}) and the gas phase mass transfer coefficient (k_g) are close under 20 and 50 °C, but the liquid phase mass transfer coefficient under 20 °C is only half value of that under 50 °C. The reason for this phenomenon is that the Henry’s coefficient of CO₂ drops from

3.81×10^{-10} mol/($\text{cm}^3 \cdot \text{Pa}$) under 20 °C to 1.92×10^{-10} mol/($\text{cm}^3 \cdot \text{Pa}$) under 50 °C. Although the gas phase mass transfer coefficient k_g grows with temperature owing to the increasing gas diffusion coefficient, the mass transfer process is controlled by liquid phase. On the premise that the gas phase mass transfer resistance is negligible, increasing temperature is beneficial for CO_2 absorption in the front half of the temperature range. So, the optimum temperature for the absorption reaction is 35 °C.

4.4 Mass transfer process

As shown in Figure 9, the absorption process within $\text{CO}_2\text{-H}_2\text{O-Mg(OH)}_2$ system is a complex combination containing physical dissolution and series of chemical reactions. The whole process can be briefly described as follows: the CO_2 molecules in the gas phase are dissolved in water and ionized to form HCO_3^- and CO_3^{2-} , meanwhile, the Mg(OH)_2 solid particles dissolve and ionize to form Mg^{2+} and OH^- in the liquid phase. The reactions occur at a plane in the liquid at a position close to the

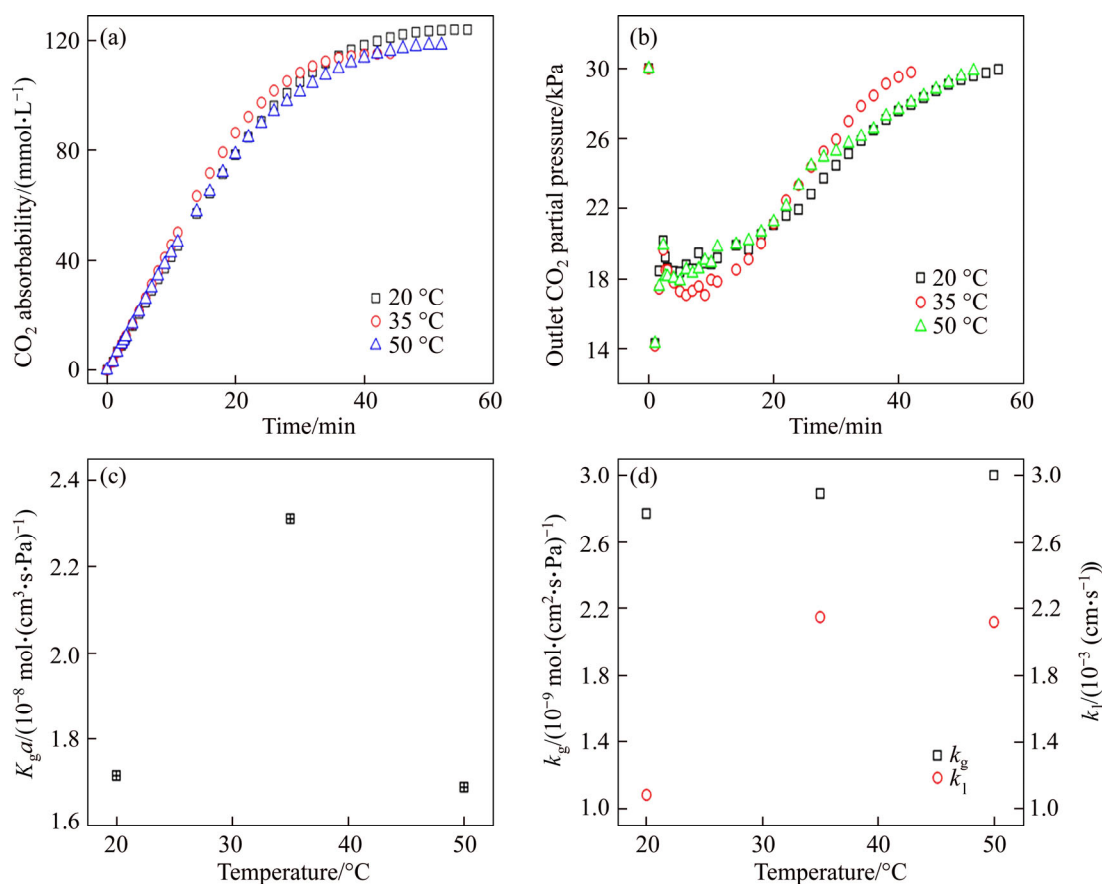


Figure 8 Absorption of CO_2 under 30% CO_2 , 0.1 mol/L Mg(OH)_2 conditions at different temperatures: (a) CO_2 absorption capacity; (b) Outlet CO_2 partial pressure; (c) Volumetric mass transfer coefficient; (d) Gas/liquid phase mass transfer coefficients

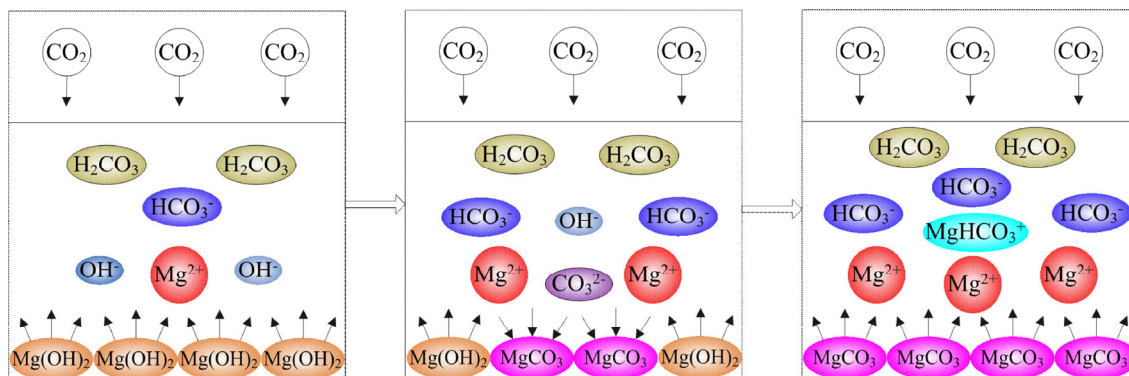


Figure 9 Absorption mechanism of $\text{CO}_2\text{-H}_2\text{O-Mg(OH)}_2$ system

gas-liquid interface as these ions reach the reaction zone. As the absorption proceeds, $\text{Mg}(\text{OH})_2$ particles are gradually converted into MgCO_3 crystals and the pH value drops accordingly. When the active surface of $\text{Mg}(\text{OH})_2$ (the surface where $\text{Mg}(\text{OH})_2$ is directly in contact with water) is consumed, the MgCO_3 crystals begin to dissolve and continue to react with CO_2 , to form the highly soluble $\text{Mg}(\text{HCO}_3)_2$. The higher the ratio of $\text{Mg}(\text{HCO}_3)_2$ in the final product, the better the subsequent desorption. However, as the absorption process progresses, the Mg^{2+} and HCO_3^- accumulated in the solution gradually increase. On the one hand, the ionization equilibrium of HCO_3^- and CO_3^{2-} limits the continued dissolution of CO_2 gas; on the other hand, Mg^{2+} accumulated in the environment with high carbonate ion concentration can easily reach the solubility product of MgCO_3 with CO_3^{2-} . The final product is a mixture of magnesium carbonate crystal and magnesium bicarbonate solution, in which the ratio of HCO_3^- to MgHCO_3^+ is about 3:1, which can be increased with temperature.

Mass transfer resistance is the reciprocal of mass transfer coefficient, enhanced absorption mass transfer is equivalent to reduced mass transfer resistance. It can be used to define where the rate determining step lies. According to the formula of modeling process, k_g is a function of temperature, pressure, gas types, gas-liquid fluid properties, surface gas velocity and dimensions of bubble

column, which is mainly affected by temperature. k_g ranges from 2.20×10^{-9} mol/($\text{cm}^3 \cdot \text{s} \cdot \text{Pa}$) at 20 °C to 3.0×10^{-9} mol/($\text{cm}^3 \cdot \text{s} \cdot \text{Pa}$) at 50 °C. Compare the experimental data, liquid phase mass transfer resistance takes up the overwhelming majority in CO_2 - H_2O - $\text{Mg}(\text{OH})_2$ system, and gas phase mass transfer resistance occupies less than 1% of the overall mass transfer resistance. The delay of liquid phase mass transfer means that gas concentration has little effect on gas-liquid mass transfer. Results of low concentration of CO_2 gas prove that gas concentration has little influence on mass transfer coefficients. High concentration of CO_2 gas is not conducive to absorption because it leads to fast deposition of $\text{MgCO}_3 \cdot 3\text{H}_2\text{O}$ crystals on the surfaces of unreacted $\text{Mg}(\text{OH})_2$ particles which reduces the utilization ratio of magnesium hydroxide, and high CO_3^{2-} ion concentration limits the dissolution of MgCO_3 to absorb CO_2 continually. The deactivation process of $\text{Mg}(\text{OH})_2$ particles is illustrated in Figure 10.

This conclusion can be also verified by comparing the mass transfer coefficients of control group (25 °C, 0.1 mol/L $\text{Mg}(\text{OH})_2$, 15% CO_2) with other groups under different temperatures. Despite the fact that the partial pressure on CO_2 of control group under 25 °C has only half that of other groups, the mass transfer coefficients fit well with the change of temperature, and the results are consistent with previous studies [15, 30]. Therefore, increasing the concentration of $\text{Mg}(\text{OH})_2$ slurry and

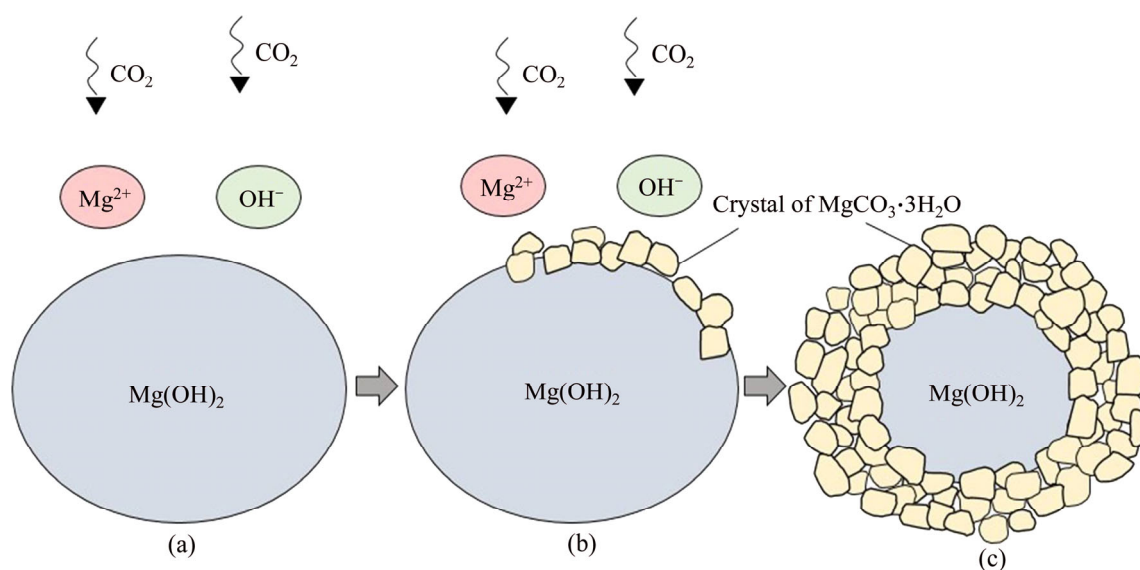


Figure 10 Illustration of $\text{Mg}(\text{OH})_2$ particles under high CO_2 concentration conditions: (a) Unreacted $\text{Mg}(\text{OH})_2$ particle; (b) Particle surface partially deactivated by covering of $\text{MgCO}_3 \cdot 3\text{H}_2\text{O}$ crystals; (c) Unreacted $\text{Mg}(\text{OH})_2$ particle totally covered by $\text{MgCO}_3 \cdot 3\text{H}_2\text{O}$ crystals

reaction temperature can effectively reduce the resistance of liquid phase mass transfer.

5 Conclusions

This study has proposed a computational model of gas-liquid mass transfer coefficients in CO₂-H₂O-Mg(OH)₂ system based on penetration theory. The mass transfer coefficients are functions of liquid properties, Henry's law constant, hydrodynamic parameters, diffusion coefficients, bubble characteristics and gas holdup. Although there is enhancement of chemical reaction, the mass transfer process is liquid-controlled. The liquid phase mass transfer resistance occupies more than 99% of the overall mass transfer resistance. The mass transfer process is mainly influenced by slurry concentration and reaction temperature. Volumetric mass transfer coefficient $K_g a$ and liquid side mass transfer coefficient K_l increase with the concentration of Mg(OH)₂ slurry, then the trends remain constant when the concentration is over 0.05 mol/L. $K_g a$ increases in low temperature range (20–35 °C), while the trends reverse in high temperature range (35–50 °C). k_l reaches the maximum value at 35 °C, the reason for high k_l at 50 °C is the rapid drop of Henry's law constant of CO₂, gas concentration has indirect effects on absorption. To be precise, mass transfer coefficients are stable in both low CO₂ concentration range (10%–15%, volume fraction) and high CO₂ concentration range (20%–30%, volume fraction) respectively. High CO₂ concentration gas is not conducive to absorption because it leads to fast deposition of MgCO₃·3H₂O crystals which cover the surfaces of unreacted Mg(OH)₂ particles, and high CO₃²⁻ ion concentration limits the dissolution of MgCO₃ to absorb CO₂ continually, but increasing CO₂ concentration is helpful to reduce equilibrium time. Concentration of 0.05 mol/L Mg(OH)₂, 15% CO₂ and operation temperature at 35 °C are recommended for CO₂ absorption.

Nomenclatures

a Surface area per unit volume, cm²/cm³
 C_i CO₂ concentration at the gas-liquid interface, mol/L
 C_{average} Average CO₂ concentration in the gas bubble, mol/L

C_{cl} Equilibrium CO₂ concentration in the bulk liquid, mol/L
 d_0 Diameter of the initial bubble, mm
 d_b Sauter mean bubble diameter of bubble swarms, mm
 d_h Nozzle diameter, mm
 D Diameter of bubble column reactor, m
 D_g Diffusion coefficient in bulk gas, cm²/s
 D_l Diffusion coefficient in bulk liquid, cm²/s
 g Gravitational acceleration, m/s²
 H_{CO_2} Henry's law constant of CO₂, mol/(L·Pa)
 h Height of liquid column, m
 K_g Overall mass transfer coefficient, mol/(cm²·s·Pa)
 K_l Overall mass transfer coefficient, cm/s
 k_g Gas side mass transfer coefficient, mol/(cm²·s·Pa)
 k_l Liquid side mass transfer coefficient, cm/s
 M_a, M_b Molecular mass, kg/kmol
 N_a Total amount of absorbed CO₂, mol
 N Total amount of inlet gas, mol
 N_{Sh} Sherwood number, $k_g d_b / D_g$
 N_{Fo} Fourier number, $D_g \theta / d_b^2$
 N_{Pe} Peclet number, $d_b^2 / D_g \theta$
 P_{average} Average CO₂ partial pressure in the gas bubble, Pa
 P_{in} Inlet CO₂ partial pressure, Pa
 P_{out} Outlet CO₂ partial pressure, Pa
 P_{cl}^* Equilibrium CO₂ partial pressure at the gas-liquid interface, Pa
 P_i CO₂ partial pressure at the gas-liquid interface, Pa
 R Gas constant, $R=8.314472 \times 10^6$ cm³·Pa/(K·mol)
 r_a Mass transfer rate, mol/(cm³·s)
 r_B Bubble radius, mm
 T Temperature, K
 $T_{\text{cA}}, T_{\text{cB}}$ Critical temperature, K
 t Equilibrium time, s
 U_g Superficial gas velocity, m/s
 U_t Terminal rising velocity of bubble swarms, m/s
 V Volumetric gas flow rate through the nozzle, m³/s
 $V_{\text{cA}}, V_{\text{cB}}$ Critical volume, cm³/mol

V_l	Liquid volume of the gas-liquid mixture, m^3
V_g	Gas volume of the gas-liquid mixture, m^3
y_1	CO ₂ mole fraction of inlet gas
y_2	CO ₂ mole fraction of outlet gas
σ	Surface tension, N/m
ε	Gas holdup
η	Absorption efficiency
θ	Characteristic contact time of penetration theory, s
ν	Kinematic viscosity, m^2/s
ρ	Density, kg/m^3
τ	Any time moment

References

- [1] SKREIBERG A, SKREIBERG Ø, SANDQUIST J, SØRUM L. TGA and macro-TGA characterisation of biomass fuels and fuel mixtures [J]. *Fuel*, 2011, 90(6): 2182–2197.
- [2] HANAOKA T, INOUE S, UNO S, OGI T, MINOWA T. Effect of woody biomass components on air-steam gasification [J]. *Biomass & Bioenergy*, 2005, 28(1): 69–76.
- [3] RUBIN E S, CHEN C, RAO A B. Cost and performance of fossil fuel power plants with CO₂ capture and storage [J]. *Energy Policy*, 2007, 35(9): 4444–4454.
- [4] ABU-ZAHRA M R M, SCHNEIDERS L H J, NIEDERER J P M, FERON P H M, VERSTEEG G F. CO₂ capture from power plants Part I. A parametric study of the technical performance based on monoethanolamine [J]. *International Journal of Greenhouse Gas Control*, 2007, 1(1): 240–249.
- [5] CHENG L, LI T, KEENER T C, LEE J Y. A mass transfer model of absorption of carbon dioxide in a bubble column reactor by using magnesium hydroxide slurry [J]. *International Journal of Greenhouse Gas Control*, 2013, 17: 240–249.
- [6] HUANG Hou-ping, CHANG S G, DORCHAK T. Method to regenerate ammonia for the capture of carbon dioxide [J]. *Energy and Fuels*, 2002, 16: 904–910.
- [7] VALENTI G, BONALUMI D, MACCHI E. A parametric investigation of the chilled ammonia process from energy and economic perspectives [J]. *Fuel*, 2012, 101: 74–83.
- [8] YAN Li-yun, LU Xiao-feng, WANG Quan-hai, KANG Yin-hu, XU Jie, CHEN Ye. Research on sulfur recovery from the byproducts of magnesia wet flue gas desulfurization [J]. *Applied Thermal Engineering*, 2014, 65(1, 2): 487–494.
- [9] KRISHNA R, van BATEN J M. Mass transfer in bubble columns [J]. *Catalysis Today*, 2003, 79: 67–75.
- [10] ZHAO Bin, WANG Jin-fu, YANG Wei-guo, JIN Yong. Gas-liquid mass transfer in slurry bubble systems: I. Mathematical modeling based on a single bubble mechanism [J]. *Chemical Engineering Journal*, 2003, 96(1–3): 23–27.
- [11] CHEN Pao-chi, HUANG Chen-huai, SU Ting, CHEN H, YANG Ming-wei, TSAO J. Optimum conditions for the capture of carbon dioxide with a bubble-column scrubber [J]. *International Journal of Greenhouse Gas Control*, 2015, 35: 47–55.
- [12] PASHAEI H, GHAEMI A, NASIRI M. Experimental investigation of CO₂ removal using Piperazine solution in a stirrer bubble column [J]. *International Journal of Greenhouse Gas Control*, 2017, 63: 226–240.
- [13] YANG Wei-guo, WANG Jin-fu, ZHAO Bin, JIN Yong. Gas-liquid mass transfer in slurry bubble systems: II. Verification and simulation of the model based on the single bubble mechanism [J]. *Chemical Engineering Journal*, 2003, 96: 29–35.
- [14] AZBEL D. Two phase flows in chemical engineering [M]. Cambridge: Cambridge University Press, 2009: 174–178.
- [15] JAKOBSEN H A, LINDBORG H, DORAO C A. Modeling of bubble column reactors: Progress and limitations [J]. *Industrial & Engineering Chemistry Research*, 2005, 44(14): 5107–5151.
- [16] ALVES S S, MAIA C I, VASCONCELOS J M T, SERRALHEIRO A J. Bubble size in aerated stirred tanks [J]. *Chemical Engineering Journal*, 2002, 89(1–3): 109–117.
- [17] KULKARNI A A, JOSHI J B. Bubble formation and bubble rise velocity in gas-liquid systems: A review [J]. *Industrial & Engineering Chemistry Research*, 2005, 44(16): 5873–5931.
- [18] AKITA K, YOSHIDA F. Bubble size, interfacial area, and liquid-phase mass transfer coefficient in bubble columns [J]. *Industrial & Engineering Chemistry Process Design and Development*, 2002, 13: 84–91.
- [19] MARTÍN M, MONTES F J, GALÁN M A. Bubbling process in stirred tank reactors I: Agitator effect on bubble size, formation and rising [J]. *Chemical Engineering Science*, 2008, 63(12): 3212–3222.
- [20] BOYER C, DUQUENNE A M, WILD G. Measuring techniques in gas-liquid and gas-liquid-solid reactors [J]. *Chemical Engineering Science*, 2002, 57(16): 3185–3215.
- [21] GRUND G, SCHUMPE A, DECKWER W D. Gas-liquid mass transfer in a bubble column with organic liquids [J]. *Chemical Engineering Science*, 1992, 47(13, 14): 3509–3516.
- [22] GADDIS E S, VOGELPOHL A. Bubble formation in quiescent liquids under constant flow conditions [J]. *Chemical Engineering Science*, 1986, 41(1): 97–105.
- [23] AKITA K, YOSHIDA F. Gas holdup and volumetric mass transfer coefficient in bubble columns [J]. *Industrial & Engineering Chemistry Process Design and Development*, 1973, 12(1): 76–80.
- [24] YANG G Q, DU B, FAN L S. Bubble formation and dynamics in gas-liquid-solid fluidization: A review [J]. *Chemical Engineering Science*, 2007, 62(1, 2): 2–27.
- [25] MENDELSON H D. The prediction of bubble terminal velocities from wave theory [J]. *AIChE Journal*, 1967, 13(2): 250–253.
- [26] JIN Hai-bo, YANG Suo-he, HE Guang-xiang, LIU De-lin, TONG Ze-min, ZHU Jian-hua. Gas-liquid mass transfer characteristics in a gas-liquid-solid bubble column under elevated pressure and temperature [J]. *Chinese Journal of Chemical Engineering*, 2014, 22(9): 955–961.
- [27] DECKWER W D, BURCKHART R, ZOLL G. Mixing and mass transfer in tall bubble columns [J]. *Chemical Engineering Science*, 1974, 29(11): 2177–2188.

- [28] SUH I S, SCHUMPE A, DECKWER W D, KULICKE W M. Gas-liquid mass transfer in the bubble column with viscoelastic liquid [J]. Canadian Journal of Chemical Engineering, 1991, 69(2): 506–512.
- [29] XIAO Y, LOW B T, HOSSEINI S S, CHUNG T S, PAUL D R. The strategies of molecular architecture and modification of polyimide-based membranes for CO₂ removal from natural gas-A review [J]. Progress in Polymer Science, 2009, 34(6): 561–580.
- [30] KRAAKMAN N J R, ROCHA-RIOS J, LOOSDRECHT M C M. Review of mass transfer aspects for biological gas treatment [J]. Applied Microbiology and Biotechnology, 2011, 91: 873–886.

(Edited by FANG Jing-hua)

中文导读

鼓泡反应器中氢氧化镁浆液脱碳的气液传质研究

摘要：氢氧化镁被认为是燃煤电厂和生物质气脱碳的潜在溶剂。本文描述了浆态床鼓泡反应器中 CO₂-H₂O-Mg(OH)₂ 体系的化学作用和传质机理，建立了可靠的计算模型。利用实验方法和软件辅助仿真，得到了总传质系数和单位体积表面积。结果表明：Mg(OH)₂ 浆体吸收 CO₂ 的传质过程主要是液膜控制过程，其中浆液浓度和反应温度是影响气泡塔反应器体积传质系数和液相传质系数的主要因素。高浓度的二氧化碳对其吸收有不利影响，因其导致 MgCO₃·3H₂O 晶体快速沉积在未反应的 Mg(OH)₂ 颗粒表面，降低了氢氧化镁的利用率。同时，高 CO₃²⁻ 离子浓度限制了 MgCO₃ 的溶解，使其不能持续吸收 CO₂。建议二氧化碳捕集系统的反应条件为氢氧化镁溶液浓度 0.05 mol/L，二氧化碳体积浓度 15%，反应温度 35 °C。

关键词：传质过程；CO₂ 捕集；氢氧化镁；鼓泡塔